Geosfera Indonesia
p-ISSN 2598-9723, e-ISSN 2614-8528
available online at : https://jurnal.unej.ac.id/index.php/GEOSI
Vol. 7 No. 3, December 2022, 264-276

https://doi.org/10.19184/geosi.v7i3.30169 **Research Article**

Performance of UAV Image for Flood Mapping with 2 Dimensional Model in Kaliputih River, Panti District

Icha Derka, Entin Hidayah *, Gusfan Halik
Department of Civil Engineering, University of Jember, Jember, 68121, Indonesia
*Corresponding author, Email address : entin.teknik@unej.ac.id

ARTICLE INFO

Article history

Received :
11 February 2022

Revised :
16 July 2022

Accepted :
1 June 2022

Published :
24 December 2022

ABSTRACT

In January 2006, the flash flood in Panti Sub-district was a national disaster, causing damage to building infrastructure and fatalities. From this incident, it is necessary to have flood mitigation by providing a map of the distribution of flood inundation using a 2D hydraulic model to provide information regarding the extent of flood inundation in the study area. Due to the limited DEM data for 2D modeling, it is necessary to use UAV images to provide a DSM with good and higher resolution. This study aims to assess the performance of 2D flood modeling results using HEC-RAS equipped with RAS Mapper through UAV processing as input. There are 21 GCP in the study area as an increase in accuracy, the RMSE value in the horizontal direction is 0.3853m, and the vertical direction is 0.1836m. From the CE90 accuracy test results for a horizontal accuracy of 0.58m and LE90 for a vertical accuracy of 0.30m, it can be concluded that the map accuracy test meets the 1:2500 scale. Terrain maps are input to HEC-RAS; selected meshes are 5x5m and 2x2m. The modeling results can show the inundation depth in each GCP from the min-max depth. The model calibration shows an RMSE value of 0.183, while the flood depth validation shows an RMSE value of 0.13. In other words, modeling can represent the distribution of flood inundation in the study area and provide benefits for the community to be more alert in the event of a flood in the coming year.

Keywords : UAV; GCP; DSM; HEC-RA; Flood mapping

1. Introduction

Jember Regency, precisely in Panti Subdistrict, is one of the flood-prone areas; it can be seen on the disaster-prone map of the Jember Regency by BPBD. In 2006, a flash flood had occurred in Panti District on January 1. This incident resulted in around thirty-one people dead and seven people missing, 120 houses, rice fields, and plantations were damaged, and bridges were cut (Khusniani, 2006). Flash floods resulted in fatalities and damage to some facilities and infrastructure. According to BPBD, Panti Sub-district was the area most severely affected by flash floods compared to 10 other sub-districts, which was due to the lack of a disaster information system. In addition, in 2011, the Panti was hit by another flood, precisely on Friday, March 4, 2011, which damaged roads and injured four people (Seno, 2011). In 2016, to be precise, on Sunday, February 4, there was an overflow of river water in Panti District, which damaged roads and clean waterways (Luqmanto, 2016).

In 2019, the Head of the Emergency and Logistics Division of BPBD said that the water discharge of the Kaliputih river increased to 3m, causing hundreds of residents to flee to safer places. Moreover, on Sunday, January 26, 2020, there was a flood in Panti District, which inundated residential areas and agricultural land, making it difficult to evacuate (Simbolon, 2020). On January 28, 2022 BPBD recorded flood events in several sub-districts, one of which was in Panti Sub-district which submerged two residents' houses.

From the various events, mitigation efforts are needed by providing a map of the distribution of flood inundation using a 2D hydraulic model to provide information regarding the extent of flood inundation in the study area (Ongdas et al., 2020). The modeling required terrain input in DEM data (Tunas et al., 2019). However, the lack of topographic data in the study area makes flood modeling require the use of UAV images (Karamuz et al., 2020), because the results of UAV processing can produce a good DSM (Bhandari et al., 2015). For this reason, UAV image technology is very support in this study, which can produce high-resolution data that is smaller than 1m.

The use of UAV imagery in previous studies has resulted in high accuracy on high-resolution maps. Orthophoto data was used to test the accuracy of x,y, and DSM, which was converted to DTM to test the accuracy of the z value (Taufik et al., 2020). To get a good level of accuracy, it is necessary to plan GCP points that are spread evenly in the study area (Gindraux et al., 2017). GCP points must be clear, easily visible, and not easily changed. Besides that, the GCP is in the WGS-84 datum coordinate system and is made of non-destructive materials with contrasting colors (National Land Agency, 2017). Based on the success of UAV images in producing high resolution, this study uses UAV images with a resolution smaller than 50cm/pixel according to BIG for flood hazard mapping.

This study aims to perform flood modeling using HEC-RAS equipped with RAS Mapper. In general, the advantages of HEC-RAS 2D itself are that it can simulate flooding in various flood scenarios (Ongdas et al., 2020) and estimate the level of flood depth. The results of UAV processing are used as terrain input in HEC-RAS (Mourato et al., 2017), and the discharge value is also inputted so that it can produce flood inundation modeling through simulation of the desired scenario (Kim et al., 2020). In this way, the flood modeling map produced will be much better at representing the geometry of the Kaliputih River in Kemiri Village, Panti-East Java District. Then the results of flood inundation modeling can be used to inform the surrounding community about vulnerable areas and the distribution of flood inundation.

The location of Kaliputih was chosen in Panti District because there was a large flash flood in 2006 and resulted in many fatalities in this area. In addition, almost every year, floods occur in the study area. The absence of an early warning system at the study site results in a lack of knowledge among the residents about anticipating hazards. Therefore, flood mitigation efforts by providing a map of the distribution of flood inundation using a 2D hydraulic model through the results of UAV processing need to be made in the study area to provide information to the public regarding the distribution of flood inundation.

2. Methods

The research process is divided into three stages: the first stage of collecting topographic data to obtain a terrain map, the second stage of HEC-RAS 2D modeling is to obtain the distribution of flood inundation and the third stage of modeling validation for the first and second stages of the process.

2.1 Study Area

The location of the research was carried out in the Kaliputih Subwatershed, which is included in the Bedadung watershed, and has an area of 27.32 km² (consisting of 21.92 km² of the forest, 0.02 km² of vacant land, 0.59 km² of settlements, 0.05 km² of irrigated rice fields, 1.98 km² of shrubs, 2.10 km² of gardens and 0.66 km² of fields). The selected area is the Kaliputih River along 3.13 km with a 3

UAV photo area. 83 km², which is used as the determination of the GCP point.

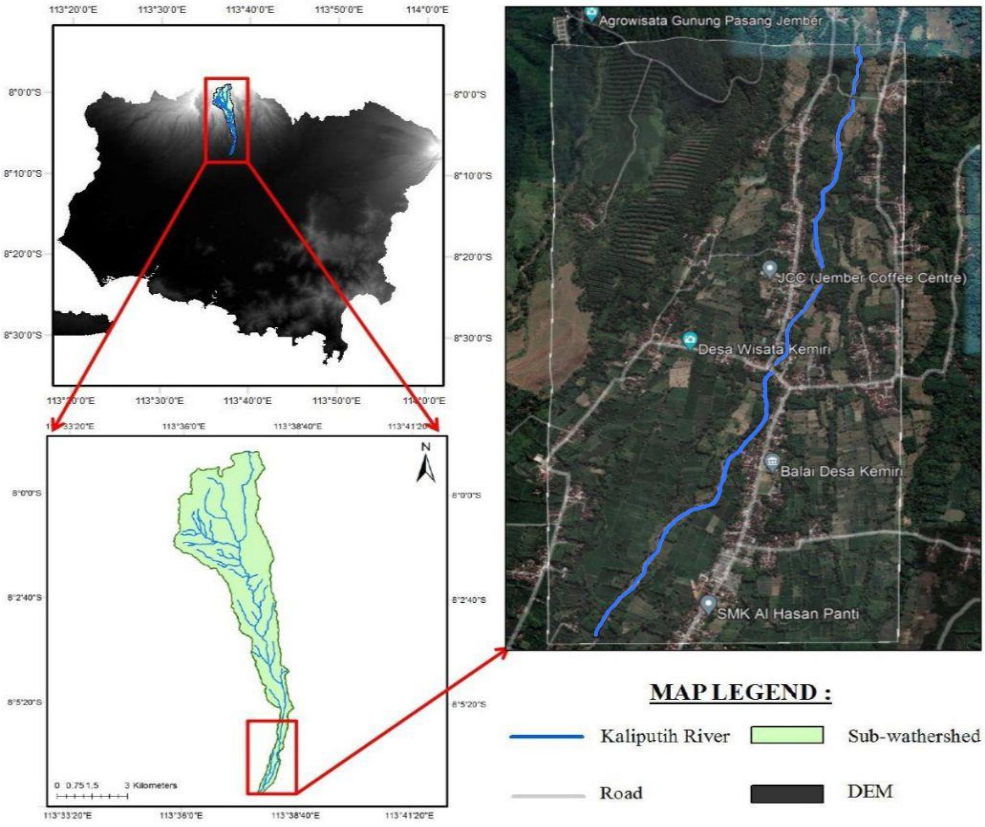

Figure 1. Study area

Topographic data collection at the case study is carried out by field survey, determining and placing GCP points as control points for UAV recording to obtain terrain maps. The discharge and water level data were obtained from PU SDA Jember in 2020 on the MAKAM DAM discharge records which were used for the model calibration process. At the same time, the field survey and the filling out the form by respondents were used to determine the distribution of floods and depth in the model validation process.

2.2 Unmanned Aerial Vehicle (UAV) Recording

Recording of study locations was carried out with the DJI Phantom 4 Pro Camera UAV as a tool for taking aerial photos. Smartphones are used to plan the placement of GPS per GCP point (via google earth) and retrieve data in the form of field photos and stationery as data recording. Aerial photography will be taken on Tuesday, November 23, 2021, until November 27, 2021, starting at 07.00 WIB - finish according to the weather conditions on the spot. UAV flights are carried out according to areas that have defined boundaries.

The determination of the UAV's flying height can be done using Pix4D_GSD_Calculator. Taking into account the target resolution, camera type, and UAV sensor. Ground Sample Distance (GSD) is obtained from equation (Elkhrachy, 2021):

$$GSD = (Sw \times H \times 100) / (Fr \times imW) \quad (1)$$

$$DW = (GSD \times imW)/100 \quad (2)$$

$$DH = (GSD \times imH)/100 \quad (3)$$

GSD is a measure of the resolution of the UAV results obtained from the comparison between values; Sw = sensor width of the camera (DJI Phantom 4 Pro Camera is 1" = 25.4 mm); H = flight altitude (maximum 120 m = 12000 cm), then divided by; Fr = Focal length of camera (24 mm resolution); imW = image width (width of the resulting image (4096 pixels). While DW = width of single image footprint on the ground (m) obtained from the multiplication value of GSD with imW per 100; and DH = height of single image footprint on the ground (m) is obtained by multiplying GSD with imH (image height = 2160 pixels) per 100. From the above equation, the GSD value is 3.10 cm/pixels, the DW value is 127 m, and the DH value is 67 m.

2.3 Ground Control Point (GCP)

Before starting aerial photography, it is necessary to define the boundaries and placement of GCP points. In its determination, the GCP must be evenly distributed and can represent the selected study area (Sanz-ablanedo & Chandler, 2018). GCP points must be clear, easily visible, and not easily changed. Besides, the GCP is in the WGS-84 datum coordinate system and is made of non-destructive materials with contrasting colors. GCP points were made by using white pylox for placement areas on paved roads. Areas located in fields or open land used blue tarpaulins and were marked with a white (O) and nailed so that they are not easy to slide and disappear (National Land Agency, 2017). The GCP used in this study was intentionally selected by considering some aspects: land conditions, access to the GCP location, land cover and minimizing GAP errors on GPS by not measuring below the slope, as well as references and GPS working concepts based on BIG tools (Stöcker et al., 2020).

Coordinates points were determined by using a GPS GeoExplorer 3000 Series Trimble. It is a GPS mapping that has an accuracy of 3m, using the L1 static observation method for 15 min, and made 2 observations at one point to show the accuracy of the observations. The determination of the height was calculated orthometrically using BIG 's geoid modeling. The limits and GCP determination can be seen in Figure 3.

Figure 2.Marking and reading of GCP points

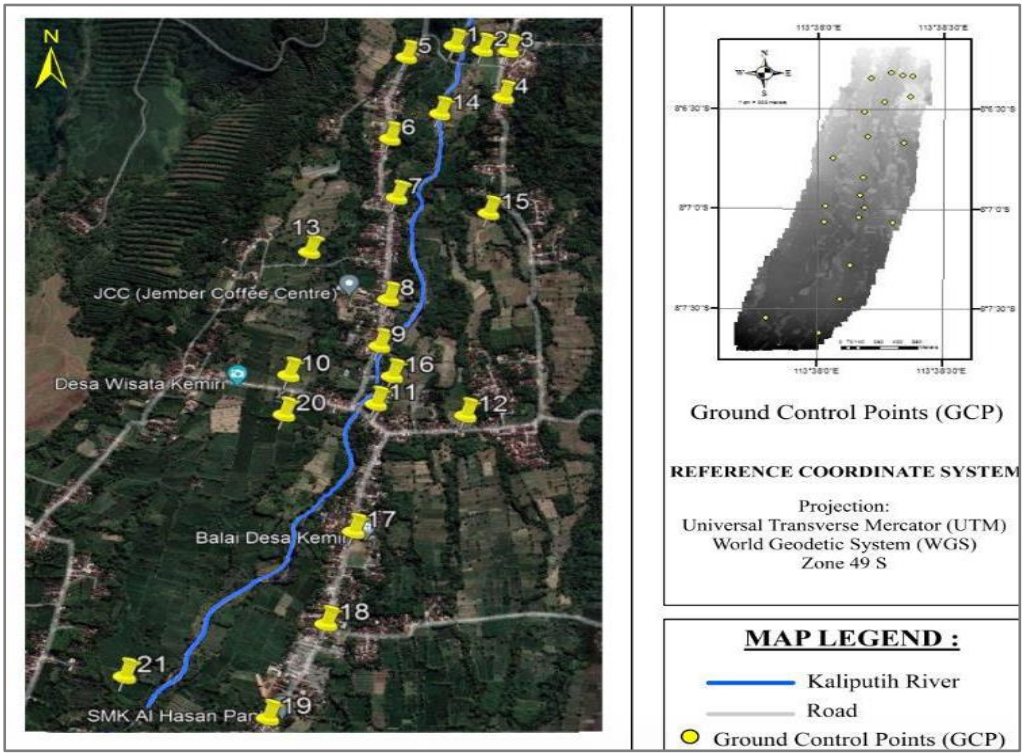

Figure 3. GCP Boundaries and Points

2.4 UAV Image Product for Generating Digital Terrain Model (DTM)

The products produced from the UAV were exported into two primary data: the Orthophoto RGB band as an interpretation of the existing appearance and DSM. The DSM data generated from the UAV still contained data errors (spikes) on the water surface. The DSM data was then improved by removing points and interpolating according to the geometric measurements of the river. In this study, DTM can be generated from the schema filtering method using a tool with the help of pix4D (Stöcker et al., 2020). The data were obtained from the rendering of Agisoft through UAV images, which were then calculated for the data accuracy assessment process (Azmi et al., 2014; Prayogo et al., 2020).

2.5 HEC-RAS Modeling

HEC-RAS was created by the Hydrologic Engineering Center (HEC), where the program is used to model flow in rivers. It was developed by the Head of the HEC-RAS Development Division, Gary W. Brunner, and Mark R. Jensen, as user interface developers. The development of HEC-RAS accommodates several model components such as analysis of permanent and non-permanent flow face profiles, sediment transport analysis, and water quality analysis (USACE, 2018). The program is equipped with RAS Mapper, which can assist in modeling the geometry, while the geometric data to be created are flow area, river, and cross-section (Harman et al., 2008; Traore et al., 2015). HEC-RAS 2D hydraulic model can provide simulation results, while the 1D model is only in the form of tables and graphs (Bailey, 2019). 2D modeling input data in the form of DEM (Digital Elevation Model) data and terrain represented by mesh cells, 2D hydraulic models are considered better than 1D models because they can show simulations and flow movements around floodplain areas (Hamdi et al., 2019). Therefore, in this study, 2D hydraulic modeling was chosen in order to show the distribution area in the floodplain area. The 2D equation can be seen in equation (4) regarding volume conservation and equation (5) regarding momentum conservation which is governed by the Saint-Venant Equation:

$$\frac{\partial Q}{\partial x} + \frac{\partial a}{\partial t} = 0 \qquad (4)$$

$$\frac{1}{A}\frac{\partial Q}{\partial t} + \frac{1}{A}\frac{\partial}{\partial x}\left(\frac{Q^2}{A}\right) + g\frac{\partial y}{\partial x} - g(So - Sf) = 0 \quad (5)$$

Where A = flow area; x = flow path distance; Q = lateral flow per unit length of the channel; g = speed of gravity; t = time; y = hydraulic depth; So = base slope; Sf = frictional slope. The method used was the reconstruction of the DSM, which was based on terrestrial measurements and reconstructed to obtain the close-actual elevation mode.

To set the 2D Flow Area mesh and brake line, several alternatives were used to get the best model performance. BC line upstream and downstream of the river was set through the geometric data menu. In the 2D inundation modeling process, the type of unsteady flow was chosen because the river flow in the study area is a natural flow that flows in an unstable/constant manner.

2.6 Model Performance Measurement

Model performance measurement is carried out in two stages: providing terrain maps by calculating data accuracy and calibrating model performance by comparing observations and modeling. Calculation of data accuracy from UAV images can be seen in equations (6-10) below (Azmi et al., 2014; Prayogo et al., 2020).

$$MSE = (\Sigma\Delta Xi^2 + \Sigma\Delta Yi^2) / n \quad (6)$$

$$RMSEr = \sqrt{\frac{1}{n}\sum_{i=1}^{n}(\Delta Xi^2 + \Delta Yi^2)} \quad (7)$$

$$RMSEz = \sqrt{\frac{1}{n}\sum_{i=1}^{n}(\Delta Zi^2)} \quad (8)$$

$$CE90 = 1{,}5175 \times RMSEr \text{ (horizontal)} \quad (9)$$

$$LE90 = 1{,}6499 \times RMSEz \text{ (vertical)} \quad (10)$$

$$RMSE = \sqrt{(X^2 - Y^2) / n} \quad (11)$$

MSE is Mean Squared Error; RMSer is Root Mean Square Error Horizontal; RMSEz is Root Mean Square Error Vertical; Xi is Number of X errors; Yi is Total Y error; Zi is Number of Z errors; n is the number of data, and CE90 is A measure of horizontal geometric accuracy defined as the radius of a circle indicating that 90% of the error is not greater than that radius, and LE90 is A measure of the vertical geometric accuracy of the distance value indicating that 90% of the altitude error is not greater than that distance. The calibration accuracy of the model performance can be calculated using equation (11) above, where RMSE is Root Mean Square Error; x is the existing condition; y is optimization, and n is the amount of data.

3. Results and Discussion

3.1 DTM Accuracy

Accuracy calculations were obtained from GPS measurement results and the results of the x,y calibration model and the z value which have been converted from ellipsoid modeling to orthometric modeling using BIG's GEOID modeling facility. This orthometric value was then used to calibrate the z value in DSM modeling (Taufik et al., 2020). The type of tool used was a GPS L1 Mapping tool without an additional antenna, so the accuracy was also low. To maximize this accuracy, repeated observations were made with two times literacy and 2 hours of observation time at each GCP point. DTM accuracy is seen from the RMSE value based on the difference in coordinate values read by GPS and UAV (Azmi et al., 2014; Villanueva & Blanco, 2019), which can be seen in equations (7) and (8). Each coordinate and the resulting RMSE value is in Table 1. For DTM, accuracy values based on map scale accuracy (Khaulan et al., 2021), can be seen in Table 2.

Table 1. Horizontal and Vertical Accuracy Test

GCP	Coordinate GPS			Coordinate UAV			WGS 84 UTM Zone 49S		
	X Longitude	Y Latitude	Z	X Longitude	Y Latitude	Z	X Error	Y Error	Z Error
1	790735.57	9103116.93	407.19	790735.83	9103116.78	407.20	0.069	0.021	0.000
2	790819.88	9103096.53	412.47	790819.55	9103096.19	412.77	0.106	0.118	0.091
3	790893.30	9103087.20	419.34	790892.94	9103086.86	419.05	0.127	0.113	0.084
4	790874.16	9102901.91	421.24	790874.11	9102901.96	421.30	0.003	0.003	0.003
5	790592.56	9103068.20	410.67	790592.98	9103068.56	410.78	0.173	0.131	0.011
6	790543.97	9102755.17	391.19	790543.71	9102754.94	390.96	0.067	0.055	0.053
7	790561.12	9102529.76	378.59	790561.41	9102529.52	378.84	0.087	0.056	0.064
8	790535.82	9102153.72	356.28	790535.61	9102153.50	356.55	0.045	0.048	0.070
9	790508.53	9101985.98	343.85	790508.88	9101985.60	343.70	0.123	0.146	0.022
10	790254.69	9101883.98	344.36	790254.91	9101883.72	344.17	0.050	0.066	0.037
11	790498.20	9101777.70	332.61	790498.38	9101777.42	332.66	0.032	0.078	0.002
12	790748.82	9101733.27	339.27	790749.10	9101733.49	339.03	0.081	0.048	0.060
13	790310.47	9102331.53	378.88	790310.20	9102331.29	378.88	0.075	0.059	0.000
14	790691.66	9102853.21	391.05	790691.53	9102852.98	391.09	0.017	0.053	0.002
15	790826.87	9102474.25	362.97	790826.52	9102474.63	362.78	0.123	0.147	0.037
16	790542.59	9101872.48	337.38	790542.27	9101872.04	337.33	0.104	0.191	0.003
17	790435.73	9101331.81	316.64	790435.57	9101332.03	316.96	0.025	0.047	0.104
18	790360.28	9101021.24	313.54	790360.55	9101021.39	313.33	0.073	0.023	0.048
19	790204.83	9100710.68	283.29	790204.51	9100711.01	283.39	0.103	0.112	0.011
20	790240.30	9101741.09	336.08	790240.46	9101741.37	336.17	0.025	0.078	0.007
21	789815.10	9100849.74	296.49	789815.22	9100849.80	296.46	0.015	0.004	0.001
Sum Square							1.52	1.60	0.71
MSE							0.15		0.03
RMSEr								0.3853	
RMSEz								0.1836	
CE90/LE90							0.58		0.30

From the calculation above, the value of RMSEr is 0.3853m and RMSEz is 0.1836m. While the standard of accuracy according to NMAS (National Map Accuracy Standard) obtained CE90 values for horizontal accuracy of 0.58m and LE90 for vertical accuracy of 0.30m. The accuracy of DTM based on BIG Regulation (Geospatial Information Agency) No. 6 of 2018 can be seen in Table 2 below.

Table 2. DTM Accuracy Based on BIG

Accuracy	Test Result	Scale Map Accuracy 1:2.500		
		Class 1 (m)	Class 2 (m)	Class 3 (m)
Vertikal (LE90)	0.30	0.5	0.75	1
Horizontal (CE90)	0.58	0.75	1.5	2.5

From the test results on the accuracy above, it can be concluded that the vertical and horizontal accuracy tests of map accuracy meet the 1:2500 scale. Both are in the order of class 1, with the maximum accuracy of the vertical accuracy test of 0.5m, while the maximum accuracy of the horizontal

accuracy test is 0.75m. Previous research regarding the accuracy of DSM using UAV imagery conducted by Khaulan et al. (2021) resulted in a CE90 of 1.474m with a map accuracy meeting a scale of 1:5000, while in this study, a CE90 result of 0.58m was obtained with a map accuracy meeting a scale of 1:2500. The difference in values in previous research is because this research has gone through the process of adding the natural neighbor interpolation method to get better results than before.

UAV imagery is considered better for representing the topography of mountainous areas, as in this study (Bhandari et al., 2015; Karamuz et al., 2020; Tsunetaka et al., 2020). Previous researchers revealed that the accuracy and reproducibility of the digital elevation model obtained through UAV-SFM (Structure From Motion) were considered better than DEMTLS (Digital Elevation Model Terrestrial Laser Scanning). Meanwhile Annis et al. (2020) through a comparison of Lidar's DEM and Tinitaly's DEM inputs, showed that the resolution of the UAV results was better, namely 15 cm-30cm, while in this study, an even better resolution of 4 cm was obtained. The map accuracy-test value will be much better if the tools used are more adequate, such as the UAV image accuracy assessment that has carried out using the DJI Mavic Pro with GPS RTK can produce a map accuracy test level that meets a scale of 1:200 (Elkhrachy, 2021). While in this study 1:2500, this is due to the limitations of tools that can affect the level of accuracy. For further research, we can use better UAVs and GPS.

3.2 Flood Distribution Map

The inundation model simulation uses HEC-RAS equipped with a RAS Mapper, inputting the terrain and discharge values. The first step to modeling in RAS Mapper is to modify the terrain raster first and then create a polygon for the boundary of the flood-affected area in the Geometric-2D Flow Area menu. After that, select the best grid using several scenarios of changing the 2D Flow Area mesh and break lines. There are several scenarios of mesh changes made from 2D flow Area 15m x 15m, break line 10m x 10m; 2D flow Area 10m x 10m, break line 7m x 7m; 2D Flow Area 10m x 10m, break line 5m x 5m; 2D flow Area 5m x 5m, break line 3m x 3m; up to 2D Flow Area 5m x 5m, break line 2m x 2m. The selected mesh is 5m x 5m for the plain inundation area (2D Flow Area) with an entire grid of 39557 grid cells. Then for the break line along the river, the selected mesh is 2m x 2m for the river area with a combined total grid of 42697 grid cells. Compute run is done to see if the 2D modeling is successful. The success or failure of the mesh scenario can be seen from the 2D modeling as a result of comparing the discharge value and water level based on the information from observations in the field. The result of the flood inundation distribution map can be seen in Figure 5, while the validation of the flood inundation depth can be seen in Table 3. Before validating the model, it is necessary to calibrate the discharge and water level observations and models, and the calibration results can be seen in Figure 4 below.

Q	Observation	Model	RMSE
32.652	1.500	1.190	0.096
45.233	1.630	1.400	0.053
50.272	1.700	1.480	0.048
55.058	1.750	1.550	0.040
56.833	1.750	1.570	0.032
59.986	1.800	1.620	0.032
70.257	1.900	1.760	0.020
81.055	2.000	1.900	0.010
86.644	2.050	1.980	0.005
104.137	2.200	2.200	0.000
	Total		0.183

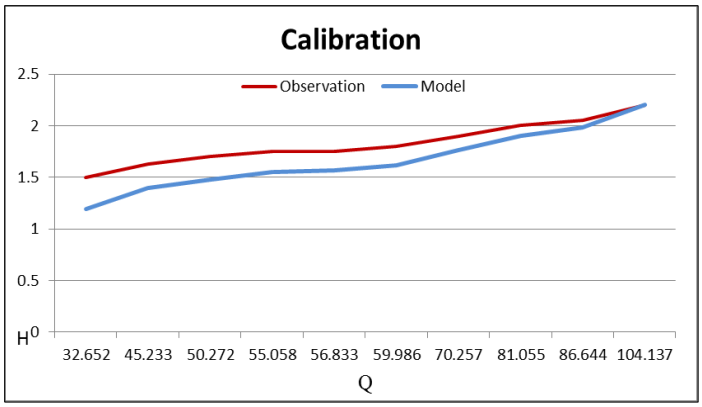

Figure 4. Calibration Results

Figure 4 shows the calibration curve of the relationship between discharge and water level. The blue curve shows the results obtained from 2D modeling, while the red curve shows the results obtained from field observations. The release of 32.652m³/second in the model shows the water level is 1.19m, while field observations are as high as 1.5m. The discharge of 45,233m³/second in the model shows a water level of 1.4m, while field observations are as high as 1.63m. The calibration results between discharge and water level observations and the model show an underestimate, and the RMSE value is close to 0, which is 0.183. In other words, the modeling can represent a map of the distribution of flood inundation in that location.

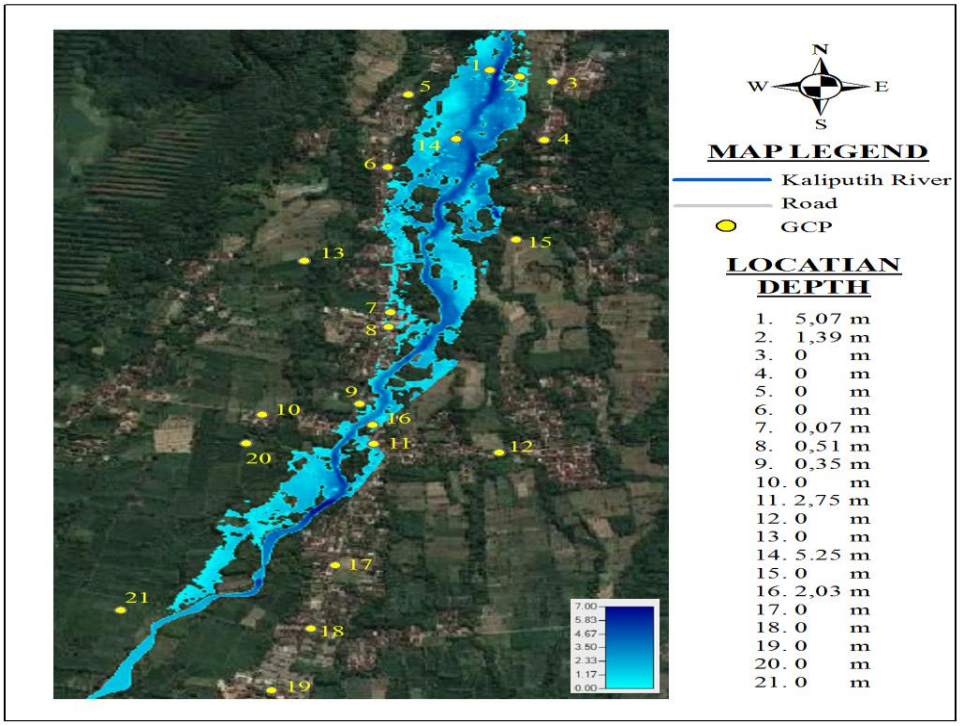

Figure 5. Flood inundation depth by HEC-RAS modeling

The results of flood mapping using a 2D hydraulic model through the HEC -RAS program resulted in a flood distribution in the study area of the Kaliputih Sub-watershed, Kemiri Village of +60.7 Ha (affected land includes settlements, rice fields, gardens, and other open lands). GCP points are used as validation points for the inundation height between the results of running modeling and the natural conditions in the study area. HEC-RAS modeling shows that GCP 1 (river area) at the time of the incident had a depth of 5.07m, point 2 (footpath near the river) was inundated to a depth of 1.49m, 7,8,9 point (road area) was flooded as high as 0.07m, 0.51m, and 0.35m. Point 11 (a market area with a concave area) was flooded to a depth of 2.75m and caused damage to bridges and market buildings at the time of the incident. Point 14 (river bed area) shows a depth of up to 5.25m, causing damage to agricultural land and plantations. Point 16 (residents' house area) offers a depth of 2.03m, causing damage to cages and buildings. Unflooded areas exist at GCP points 3-6, 10, 12-13, 15, 17-21, where the modeling shows a depth of 0m. The flood inundation depth in the modeling is different from the actual depth at each GCP. Therefore, the comparison between the natural field conditions and the modeling needs to be validated, as shown below. The method of validating the height of the 2D flood inundation was carried out by surveying and measuring signs of physical damage that can still be detected and interviewing people in the research location.

Table 3.Validation of Flood Depth

GCP	Coordinate		Inundation Height	HEC-RAS	Difference (m)	RMSE
1	790735.57	9103116.93	5 m	5.07 m	0.07	0.005
2	790819.88	9103096.53	1.4 m	1.39 m	0.01	0.000
3	790893.30	9103087.20	not flooded	not flooded	-	-
4	790874.16	9102901.91	not flooded	not flooded	-	-
5	790592.56	9103068.20	not flooded	not flooded	-	-
6	790543.97	9102755.17	not flooded	not flooded	-	-
7	790561.12	9102529.76	0.1 m	0.07 m	0.03	0.001
8	790535.82	9102153.72	0.5 m	0.51 m	0.01	0.000
9	790508.53	9101985.98	0.4 m	0.35 m	0.05	0.003
10	790254.69	9101883.98	not flooded	not flooded	-	-
11	790498.20	9101777.70	2.5 m	2.75 m	0.25	0.063
12	790748.82	9101733.27	not flooded	not flooded	-	-
13	790310.47	9102331.53	not flooded	not flooded	-	-
14	790691.66	9102853.21	5 m	5.25 m	0.25	0.063
15	790826.87	9102474.25	not flooded	not flooded	-	-
16	790542.59	9101872.48	2 m	2.03 m	0.03	0.001
17	790435.73	9101331.81	not flooded	not flooded	-	-
18	790360.28	9101021.24	not flooded	not flooded	-	-
19	790204.83	9100710.68	not flooded	not flooded	-	-
20	790240.30	9101741.09	not flooded	not flooded	-	-
21	789815.10	9100849.74	not flooded	not flooded	-	-
			Total			0.130

The RMSE value is the magnitude of the prediction error rate, while the validation is the accuracy between the observation data and the simulation results. Some of the model simulation results do not show 100% similarity with the actual situation; of course, each simulation result must have some differences or differences in values. Therefore, the RMSE value for validation can be used as a model suitability test based on the difference between the actual depth and the simulation depth of the model. The smaller the RMSE value is close to 0, the better the validation between the observed value and the modeling (Brunner et al., 2018). Mani et al. (2020) have proven and verified the performance of a calibrated and validated model through several indicators, one of which is the RMSE with a lower value and > 0, indicating that the simulation results of the model are superior and match the actual depth with the depth of the simulation results. From the validation of the flood inundation depth in Table 3, it can be seen that for areas that are not flooded, neither the field conditions nor the HEC-RAS have any difference. However, in inundated areas, there is a difference between the conditions in the field and the HEC-RAS modeling. The above inundation validation states that the RMSE value is close to 0, 0.130. In other words, the modeling can represent the inundation depth in the study area. Yalcin, (2019) have previously carried out 2D flood modeling using UAV imagery by mapping the 50-year, 100-500-year return period. However, several studies (Bailey, 2019; Elkhrachy, 2015; Mourato et al., 2017) did not perform validation tests related to the previous flooding, so the validity of the return period mapping model is still questionable.

4. Conclusion

With the topographical conditions in the study area, Unmanned Aerial Vehicle (UAV) data can provide a resolution of 4 cm/pixel for orthophoto and 12cm/pixel for DSM. The map accuracy test meets the 1:2500 scale so that the UAV results can be used as DEM input for 2D flood modeling. The limitations of GPS significantly affect the accuracy of the model. Therefore, for further research, it is

necessary to use geodetic GPS in the hope that the model's accuracy is much better. The results of the HEC-RAS modeling can show areas that are not inundated and inundation depths from < 1 m to close to conditions in the field. The RMSE value is 0.130, in other words, the performance of UAV processing as input for 2D flood modeling is considered good because the modeling can represent the distribution of flood inundation in the study area. Flood inundation mapping modeling is expected to be developed for making maps in flood disaster mitigation efforts, such as making risk maps and mapping evacuation routes in the study area. The hope is that it can provide information to the relevant agencies to pay more attention to flood-prone areas and become an early warning system that provides a sense of security for the community.

Conflict of Interests

The author states that there is no financial conflict of interest in research and writing, either individually or in group.

References

Annis, A., Nardi, F., Petroselli, A., Apollonio, C., Arcangeletti, E., Tauro, F., ... & Grimaldi, S. (2020). UAV-DEMs for small-scale flood hazard mapping. *Water*, *12*(6), 1717. https://doi.org/10.3390/w12061717.

Azmi, S. M., Ahmad, B., & Ahmad, A. (2014). Accuracy assessment of topographic mapping using UAV image integrated with satellite images Accuracy assessment of topographic mapping using UAV image integrated with satellite images. *IOP Conference Series: Earth and Environmental Science OPEN*, 1–6. https://doi.org/10.1088/1755-1315/18/1/012015.

Bailey, M. (2019). *A Comparison Between 1D and 2D Hydraulic Modeling for Bridge Replacement Projects*. INDOT Office of Hydraulics.

Bhandari, B., Oli, U., Pudasaini, U., & Panta, N. (2015). Generation of High Resolution Dsm Using UAV Images. *FIG Working Week*, *May*, 1–28.

Brunner, G. W., Sanchez, A., Molls, T., & Parr, D. A. (2018). HEC-RAS Verification and Validation Tests. US Army Corps of Engineers–Hydrologic.

Elkhrachy, I. (2021). Accuracy Assessment of Low-Cost Unmanned Aerial Vehicle (UAV) Photogrammetry. *Alexandria Engineering Journal*, *60*(6), 5579–5590. https://doi.org/10.1016/j.aej.2021.04.011.

Luqmanto G. (2016). *Dampak Banjir, Krisis Air Bersih Melanda Warga Kecamatan Panti*. Retrieved from https://rri.co.id.

Gindraux, S., Boesch, R., & Farinotti, D. (2017). Accuracy assessment of digital surface models from Unmanned Aerial Vehicles' imagery on glaciers. *Remote Sensing*, *9*(2), 1–15. https://doi.org/10.3390/rs9020186.

Hamdi, M., El Molla, D. A., & Gad, M. A. (2019). a Comparison Between 1D , 2D and Semi 2D Hydraulic Models. *Al -Azhar University Civil Engineering Research Magazine (CERM)*, *41*(4), 295–305.

Harman, C., Stewardson, M., & DeRose, R. (2008). Variability and uncertainty in reach bankfull hydraulic geometry. *Journal of Hydrology*, *351*(1–2), 13–25. https://doi.org/10.1016/j.jhydrol.2007.11.015.

Simbolon H. (2020). *Banjir Menggenangi Sejumlah Rumah Warga di Jember*. Retrieved from https://surabaya.liputan6.com.

National Land Agency. (2017). Petunjuk Teknis Pembuatan Peta Kerja dengan Menggunakan Pesawat Nirawak / Drone. *Direktorat Jendral Infrastruktur Keagrariaan Tahun 2016 Kementerian Agraria Dan Tata Ruang / Badan Pertanahan Nasional*, *02 /JUKNIS*, 1–12.

Karamuz, E., Romanowicz, R. J., & Doroszkiewicz, J. (2020). The use of unmanned aerial vehicles in flood hazard assessment. *Journal of Flood Risk Management*, *13*(4), 1–12. https://doi.org/10.1111/jfr3.12622.

Khaulan, D. W., Hidayah, E., & Halik, G. (2021). Accuracy of DSM By using Unmanned Aerial Vehicles on the downstream of Welang Riverbank, District of Pasuruan, Jawa Timur. *UKaRsT*, *5*(1), 49. https://doi.org/10.30737/ukarst.v5i1.1153.

Khusniani, K. (2006). *Catatan Kelam Bencana Alam di Indonesia*. Retrieved from https://kompaspedia.kompas.id.

Mani, V., Panda, R. K., & Pandey, V. K. (2020). Calibration and validation of HEC-RAS model for minor command in coastal region. *International Journal of Current Microbiology and Applied Sciences*, *9*(2), 664–678. https://doi.org/10.20546/ijcmas.2020.902.082.

Mourato, S., Fernandez, P., Pereira, L., & Moreira, M. (2017). Improving a DSM Obtained by Unmanned Aerial Vehicles for Flood Modelling. *IOP Conference Series: Earth and Environmental Science*, *95*(2). https://doi.org/10.1088/1755-1315/95/2/022014.

Ongdas, N., Akiyanova, F., Karakulov, Y., Muratbayeva, A., & Zinabdin, N. (2020). Application of HEC-RAS (2d) for flood hazard maps generation for yesil (ISHIM) river in kazakhstan. *Water (Switzerland)*, *12*(10), 1–20. https://doi.org/10.3390/w12102672.

Prayogo, I. P. H., Manoppo, F. J., & Lefrandt, L. I. R. (2020). Pemanfaatan Teknologi Unmanned Aerial Vehicle (UAV) Quadcopter Dalam Pemetaan Digital (Fotogrametri) Menggunakan Kerangka Ground Control Point (GCP). *Jurnal Ilmiah Media Engineering*, *10*(1), 6.

Sanz-ablanedo, E., & Chandler, J. H. (2018). Accuracy of Unmanned Aerial Vehicle (UAV) and SfM Photogrammetry Survey as a Function of the Number and Location of Ground Control Points Used. *Remote Sensing*, 1–19. https://doi.org/10.3390/rs10101606.

Seno, S. (2011). *Akses Jalan di Jember Terputus Banjir Bandang*. Retrieved from https://www.antaranews.com.

Stöcker, C., Nex, F., Koeva, M., & Gerke, M. (2020). High-quality UAV-based orthophotos for cadastral mapping: Guidance for optimal flight configurations. *Remote Sensing*, *12*(21), 1–23. https://doi.org/10.3390/rs12213625.

Taufik, M., Amiluddin, A., & Bioresita, F. (2020). Generated topographic data from UAV, for simple irrigation planning (Case study, sugar cane in Jember). *International Research Journal of Advanced Engineering and Science*, *5*(1), 245–248.

Traore, V. B., Bop, M., Faye, M., Giovani, M., Gueye, E. H. O., Sambou, H., Dione, A. N., Fall, S., Diaw, A. T., Sarr, J., & Chedikh Beye, A. (2015). Using of HEC-RAS model for hydraulic analysis of a river with agricultural vocation : A case study of the Kayanga River Basin , Senegal. *Science and Education Publishing*, *3*(5), 147–154. https://doi.org/10.12691/ajwr-3-5-2.

Tsunetaka, H., Hotta, N., Hayakawa, Y. S., & Imaizumi, F. (2020). Spatial accuracy assessment of unmanned aerial vehicle-based structures from motion multi-view stereo photogrammetry for geomorphic observations in initiation zones of debris flows, Ohya landslide, Japan. *Progress in Earth and Planetary Science*, *7*(1). https://doi.org/10.1186/s40645-020-00336-0.

Tunas, I. G., Arafat, Y., & Azikin, H. (2019). Integration of Digital Elevation Model (DEM) and HEC-RAS Hydrodynamic Model for flood routing. *IOP Conference Series: Materials Science and Engineering*, *620*(1). https://doi.org/10.1088/1757-899X/620/1/012026.

USACE. (2018). *Analyzing Flood Risk for Forecast Informed Reservoir Operations in the Russian River Watershed using HEC-WAT*. Washington: U.S. Army Corps of Engineers.

Kim V., Tantanee S., & Suparta W. (2020). GIS-based flood hazard mapping using HEC-RAS model: a case study of lower mekong river, cambodia vanthan. *Geographia technica*, *15*(1). *15*(1), 16–26. https://doi.org/10.21163/GT.

Villanueva, J. K. S., & Blanco, A. C. (2019). Optimization of Ground Control Point (GCP) configuration for Unmanned Aerial Vehicle (UAV) Survey Using Structure From Motion (SFM). *International Archives of the Photogrammetry, Remote Sensing and Spatial Information Sciences - ISPRS Archives*, *42*(4/W12), 167–174. https://doi.org/10.5194/isprs-archives-XLII-4-W12-167-2019.

Yalcin, E. (2019). Two-dimensional hydrodynamic modelling for urban flood risk assessment using unmanned aerial vehicle imagery: A case study of Kirsehir, Turkey. *Journal of Flood Risk Management*, *12*(S1), 1–14. https://doi.org/10.1111/jfr3.12499.